nature chemistry

ARTICLES

PUBLISHED ONLINE: 2 MAY 2016 | DOI: 10.1038/NCHEM.2511

# Dissipative self-assembly of vesicular nanoreactors

Subhabrata Maiti, Ilaria Fortunati, Camilla Ferrante, Paolo Scrimin and Leonard J. Prins*

**Dissipative self-assembly is exploited by nature to control important biological functions, such as cell division, motility and signal transduction. The ability to construct synthetic supramolecular assemblies that require the continuous consumption of energy to remain in the functional state is an essential premise for the design of synthetic systems with lifelike properties. Here, we show a new strategy for the dissipative self-assembly of functional supramolecular structures with high structural complexity. It relies on the transient stabilization of vesicles through noncovalent interactions between the surfactants and adenosine triphosphate (ATP), which acts as the chemical fuel. It is shown that the lifetime of the vesicles can be regulated by controlling the hydrolysis rate of ATP. The vesicles sustain a chemical reaction but only as long as chemical fuel is present to keep the system in the out-of-equilibrium state. The lifetime of the vesicles determines the amount of reaction product produced by the system.**

Nature extensively uses self-assembly to create molecular systems for the execution of biological functions[1]. This has served as an inspiration for chemists who, over the past decades, have learned how to implement self-assembly as a straightforward tool to access a large variety of functional molecular structures[2]. However, there is a fundamental difference between synthetic and natural self-assembly processes[3]. Synthetic self-assembly is typically an energetically downhill process driven by the gain in free energy on reaching the global or a local minimum in the free energy landscape, resulting in structures that are stable in time. In contrast, many natural self-assembly processes are energetically uphill and require a continuous consumption of energy to maintain assembly in the functional state[4]. This is referred to as dissipative self-assembly[5,6], and it is used by nature to gain temporal control over self-assembly processes and, in that way, regulate important biological functions, such as cell division[7], motility[8] and signal transduction[9]. Scientists are currently perceiving the importance of adding time as an extra dimension for the design of supramolecular systems with 'life-like' properties, such as autoconfiguration, self-healing and adaptability[3]. Recent examples of chemical systems that require energy to be operational (such as molecular motors[10,11], transport systems[12–14], surface gradients[15] and materials[16–19]) show that such systems indeed create an entirely new functional potential in the fields of materials science and nanotechnology[20,21].

The range of supramolecular structures obtained via out-of-equilibrium self-assembly is very limited, however, and they are currently restricted to fibres with low structural complexity[16–19]. This is in strong contrast with the enormous variety of supramolecular architectures that have been assembled under thermodynamic or kinetic control[2]. The main reason for this is that the design of dissipative molecular self-assembly processes requires the integration of an energy-consuming process, which is evidently far from trivial. Considering the higher complexity of such designs, it is therefore not surprising that no examples of dissipative supramolecular assemblies have so far been reported in which the energy consumption is actually used to control the chemical reactivity. Here, we describe a new strategy for the dissipative self-assembly of supramolecular structures and we use this strategy for the transient formation of vesicular nanoreactors that are able to sustain a chemical reaction only as long as chemical fuel is present to keep the system in the out-of-equilibrium state.

The presented strategy relies on the transient stabilization of a supramolecular assembly driven by noncovalent interactions with an additional molecule, which functions as the chemical fuel. The *in situ* consumption of the fuel leads to the loss of stabilizing interactions and, consequently, spontaneous dissociation of the assembly. Previously, we have shown that adenosine 5′-triphosphate (ATP) can be used for transient signal generation by temporarily displacing small fluorescent molecules from the surface of monolayer-protected gold nanoparticles[22]. This approach has now been exploited for the dissipative self-assembly of supramolecular structures with chemical functionality. The current methodology relies on the ability of multiple charged counterions to effectively stabilize micellar and vesicular aggregates composed of surfactants with charged head groups[23–25]. A decrease in the critical aggregation concentration (CAC) by several orders of magnitude in the presence of multivalent counterions has been reported[23]. This effect originates from the ability of a single multivalent counterion to interact simultaneously with multiple surfactant molecules, which is highly favourable from an entropic point of view. Considering that a similar multivalent effect was also at the origin of our previous work[22,26], we began our studies by exploring the ability of ATP to stabilize aggregates formed by surfactant $C_{16}$**TACN·Zn$^{2+}$** (Fig. 1a). This surfactant contains the identical 1,4,7-triazacyclononane·$Zn^{2+}$ (**TACN·Zn$^{2+}$**) head group as present in the previous nanoparticle system, but attached instead to an apolar $C_{16}$ chain.

The aggregation behaviour of $C_{16}$**TACN·Zn$^{2+}$** alone was studied by titrating increasing amounts of the surfactant to an aqueous solution buffered at pH 7.0 containing the fluorescent apolar probe 1,6-diphenyl-1,3,5-hexatriene (**DPH**, 2.5 μM, $\lambda_{ex} = 355$ nm, $\lambda_{em} = 428$ nm). This probe is solubilized by the apolar compartment of the aggregates, leading to an increase in fluorescence intensity after the CAC has been reached (Fig. 1b). The determined CAC value of around 100 μM, confirmed by UV–vis measurements, compares well to that of a related system reported previously (Supplementary Figs 4 and 5)[27]. Dynamic light scattering (DLS) measurements performed at a surfactant concentration of 200 μM

Department of Chemical Sciences, University of Padova, Via Marzolo 1, 35131 Padova, Italy. *e-mail: leonard.prins@unipd.it

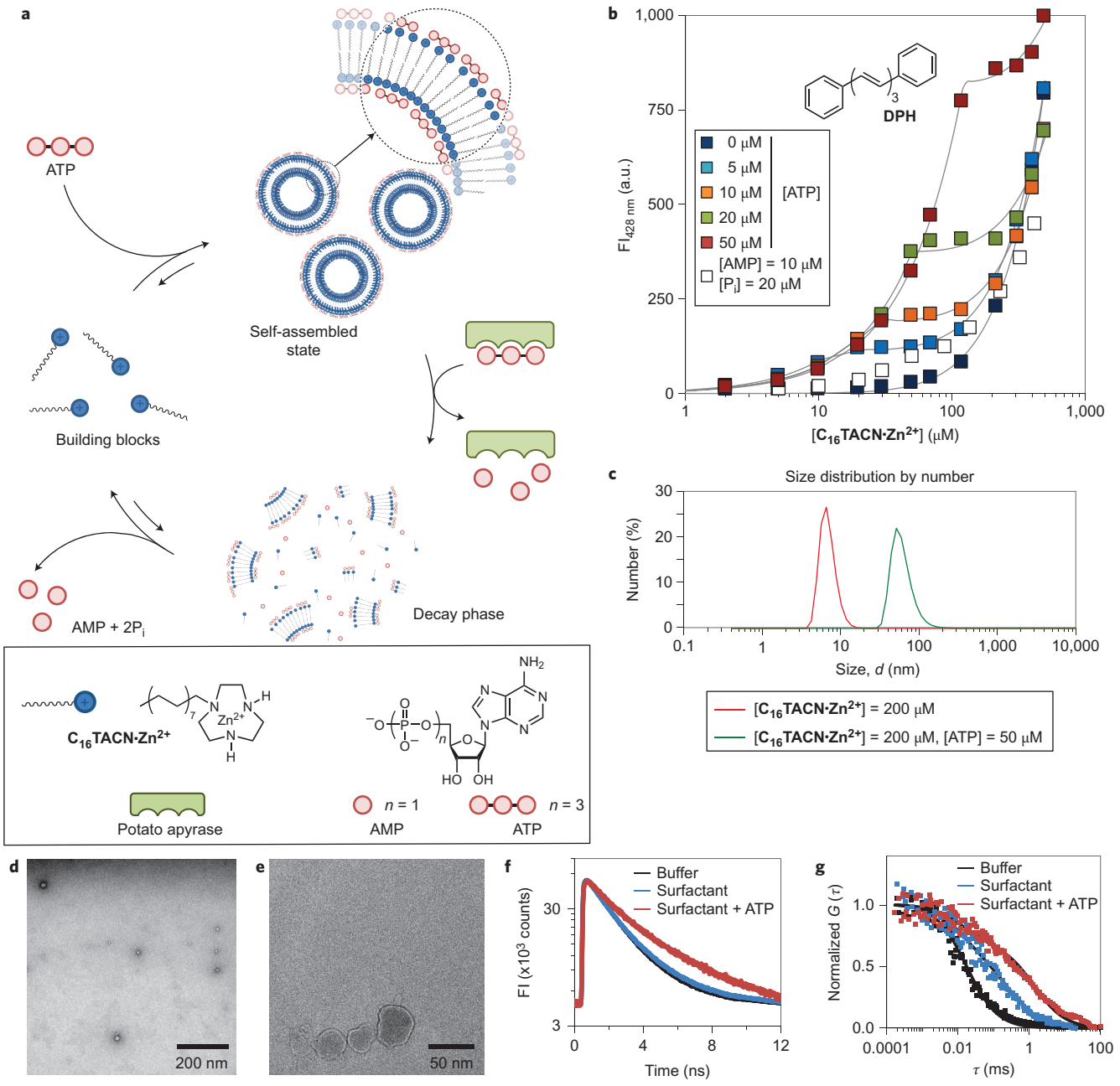


**Figure 1 | Formation and characterization of vesicles. a**, Schematic representation of the dissipative self-assembly of vesicles. **b**, Fluorescence intensity (FI) at 428 nm as a function of the concentration of $C_{16}TACN{\cdot}Zn^{2+}$ added to an aqueous buffer solution with different concentrations of ATP (0–50 μM) or AMP (10 μM) + $P_i$ (20 μM) in the presence of **DPH** (2.5 μM) as the fluorescent probe. Experimental conditions: HEPES (5 mM, pH 7.0), $T$ = 37 °C, excitation wavelength = 355 nm, slit width (ex/em) = 5/10 nm. The lines represent the best fit to model T (see Supplementary Information, page 19). **c**, Hydrodynamic diameter of the aggregates in the absence and presence of ATP measured by DLS in aqueous buffer solution (HEPES, 5 mM; pH 7.0). **d**, TEM image of vesicles with [$C_{16}TACN{\cdot}Zn^{2+}$] = 25 μM and [ATP] = 6 μM (stained with 2% uranyl acetate solution). Scale bar, 200 nm. **e**, Cryo-TEM image of vesicles with [$C_{16}TACN{\cdot}Zn^{2+}$] = 200 μM and [ATP] = 50 μM. Scale bar, 50 nm. **f**, Time-domain intensity decay of C153 in aqueous buffer, [$C_{16}TACN{\cdot}Zn^{2+}$] = 25 μM and vesicles with [$C_{16}TACN{\cdot}Zn^{2+}$] = 25 μM and [ATP] = 6 μM, excited by a 400 nm laser (HEPES, 5 mM, pH 7). **g**, Normalized FCS curves of C153 in aqueous buffer solution, micelles with [$C_{16}TACN{\cdot}Zn^{2+}$] = 200 μM and vesicles with [$C_{16}TACN{\cdot}Zn^{2+}$] = 200 μM and [ATP] = 50 μM. Solid lines are fits.

yielded a hydrodynamic diameter of 5.9 ± 1.3 nm, indicating that $C_{16}TACN{\cdot}Zn^{2+}$ aggregates into micelles (Fig. 1c).

A completely different behaviour was observed when the titrations were repeated in the presence of ATP at different concentrations (5–50 μM; Fig. 1b). In all cases, the fluorescence intensities started to increase at significantly lower surfactant concentrations (CAC ≈ 10 μM), but then levelled off at constant values before resuming a further increase following the curve measured in the absence of ATP (Fig. 1b). The lower CAC value shows that aggregates with higher stability are formed when ATP is present. The presence of the intermediate phase, which has an onset and fluorescence intensity that depends on the amount of ATP present, demonstrates that the concentration of ATP determines how much aggregate is formed. The titration curves were fitted to thermodynamic model T, which takes into account two equilibria: the self-association of $C_{16}TACN{\cdot}Zn^{2+}$ to form micelles and the ATP-induced association of $C_{16}TACN{\cdot}Zn^{2+}$ to form vesicles (see Supplementary Information, page 19). Fitting of the experimental curves using model T reveals

that, under these conditions, vesicles are formed under saturation conditions and that ATP and $C_{16}$TACN·$Zn^{2+}$ are present in a 1:2.5(±0.3) ratio in the aggregates. Additional titration experiments of ATP to a constant concentration of $C_{16}$TACN·$Zn^{2+}$ yielded a slightly higher ratio of ~1:3 (Supplementary Figs 6 and 7). Turbidity experiments showed that at this ratio the obtained aggregates are stable for long periods of up to 10 h (Supplementary Fig. 17). At ratios of ATP:$C_{16}$TACN·$Zn^{2+}$ higher than 1:3, aggregation was eventually observed, leading to the slow formation of precipitate, starting approximately 1 h after the addition of ATP.

The structure of the aggregates was studied by a variety of analytical techniques. DLS measurements at the same surfactant concentration as before (200 μM), but in the presence of 50 μM ATP, showed that the aggregates had a much higher hydrodynamic diameter of 62 ± 22 nm, which excluded the formation of micelles (Fig. 1c). The formation of spherical aggregates with diameters on the order of 50–100 nm was confirmed by transmission electron microscopy (TEM), cryogenic (cryo)-TEM and environmental scanning electron microscopy (ESEM) measurements (Fig. 1d,e and Supplementary Figs 10–12). In the absence of ATP, this kind of structure was not observed by TEM or ESEM. The structures visible in the TEM and cryo-TEM images all possessed a strongly contrasting outer shell attributed to the presence of $Zn^{2+}$ metal ions. An observed increase in the fluorescence lifetime $\tau$ of coumarin153 (C153, an apolar fluorophore used in the confocal microscopy studies described below) from 2.01 ± 0.01 ns to 3.03 ± 0.26 on the addition of ATP (6 μM) to a solution of C153 (0.5 μM) and surfactant (25 μM) is in agreement with the localization of the fluorophore in an apolar environment (Fig. 1f, Supplementary Fig. 14 and also Supplementary Table 1). Fluorescence correlation spectroscopy revealed a strong decrease in the diffusion coefficient from 28.2 ± 6.5 to 6.0 ± 2.3 $\mu m^2\ s^{-1}$ following the addition of ATP, corresponding to an increase in the hydrodynamic diameter from 15.8 ± 3.2 to 80 ± 34 nm (Fig. 1g and Supplementary Table 2). Altogether, these results strongly suggest that the observed aggregates are vesicles with ATP associated non-covalently with the inner and outer sides of the bilayer. The presence of an aqueous inner phase in the aggregates was confirmed by the fact that a water-soluble, cationic fluorophore (rhodamine 6G) could be entrapped in the interior (Supplementary Fig. 9).

Dissipative self-assembly requires the introduction of an additional process to release the chemical energy stored in ATP and eliminate the stabilizing interactions between ATP and $C_{16}$TACN·$Zn^{2+}$. We have previously shown that the enzyme potato apyrase is excellent for this purpose as it rapidly hydrolyses ATP into adenosine 5′-monophosphate (AMP) and two molecules of orthophosphate $P_i$ (ref. 22). Evidently, it is of crucial importance that hydrolysis products AMP and $P_i$ do not stabilize the vesicles (Fig. 1b). The fluorescence response curve of a titration of $C_{16}$TACN·$Zn^{2+}$ in the presence of AMP (10 μM) and $P_i$ (20 μM) showed just a small increase in fluorescence at surfactant concentrations above 30 μM, but at a much lower extent (eight times) than in an analogous experiment in the presence of ATP (10 μM). DLS measurements performed at significantly higher concentrations of both surfactant and AMP + $2P_i$ gave a hydrodynamic diameter of 14 ± 4 nm, which further confirmed that AMP and $P_i$ do not induce vesicle formation (Supplementary Fig. 15). It was decided to perform all further studies at a surfactant concentration below 30 μM to avoid the induction of any kind of aggregation by the hydrolysis products of ATP.

Kinetic fluorescence measurements showed a rapid increase in fluorescence intensity following the addition of ATP (3 μM) to a solution containing $C_{16}$TACN·$Zn^{2+}$ (10 μM) and DPH (2.5 μM) (Fig. 2a). In the absence of enzyme, the signal remained constant in time, indicating the stability of the vesicles under these conditions. We were pleased to observe that repeating the same experiment in the presence of different enzyme concentrations (0.02–0.15 U $ml^{-1}$) led to a nearly identical initial signal enhancement, but now followed by a gradual signal decay with a rate that depended on enzyme concentration (Fig. 2a). Kinetic model K1 was developed to obtain insight into the kinetic processes involved. Thise model takes into account reversible vesicle formation between $C_{16}$TACN·$Zn^{2+}$ and ATP and the hydrolysis of ATP through Michaelis–Menten kinetics. The fits to the experimental data show that model K1 accurately describes transient vesicle formation (solid lines in Fig. 2a). Kinetic model K1 was used to determine the half-life of the vesicles (defined as the time required to reach 50% of the fluorescence intensity in the absence of enzyme) as a function of enzyme concentration. Under these experimental conditions, half-lives ranging from 5 min (0.15 U $ml^{-1}$) to 43 min (0.02 U $ml^{-1}$) were calculated (Supplementary Fig. 28). Transient vesicle formation could also be monitored by UV–vis spectroscopy following the appearance and disappearance of turbidity (Supplementary Fig. 18). DLS measurements confirmed that these observations indeed originate from assembly formation and degradation, because a drop in the hydrodynamic diameter from 52 ± 22 nm to 17 ± 4 nm was measured for an aged solution (45 min) to which both ATP and enzyme were initially added (Supplementary Fig. 19). This end value corresponds to that observed for the surfactant in the presence of AMP + $2P_i$. The reversible nature of the process was demonstrated by performing up to seven cycles with the same sample, adding new batches of ATP each time the signal returned to the starting value (Fig. 2b). The efficiency of ATP in re-inducing vesicle formation decreased after each cycle, presumably because of the accumulation of waste products (AMP + $P_i$) in the closed reaction system. Interestingly, laser scanning confocal microscopy studies permitted direct visualization of vesicle formation and dissociation. Although the size of the aggregates falls below the resolving power of confocal microscopy, the accumulation of the C153 fluorophore in the apolar bilayer of the vesicles permitted the aggregates to be detected. Two cycles of vesicle formation and dissociation were directly visualized by recording an image every 5 s; these were then quantified by counting the number of fluorescent objects (Supplementary Information, page 25). Fluorescent objects appeared immediately after each addition of ATP, after which they gradually decreased in number (Fig. 2c,d, Supplementary Figs 20–22 and Supplementary Movie 1). In the absence of ATP, distinguishable fluorescent structures were never observed (Fig. 2d).

These experiments clearly demonstrate the transient formation of vesicles with a lifetime that can be controlled by regulating the hydrolysis rate of ATP. Compared to previously reported dissipative assemblies that all rely on covalent modification of the building blocks by a chemical fuel[14,16–20], the novelty of this approach is that ATP stabilizes the assembly through noncovalent interactions. It is of interest to note that the formation of microtubules[7] and actin filaments[8], which are some of the finest examples of dissipative natural self-assembly, also rely on the noncovalent activation of the subunits by guanosine 5′-triphosphate (GTP) and ATP, respectively. The fast 'on' and 'off' rates of the complex between surfactants and ATP allows dissipative self-assembly to occur in a kinetic regime (minutes) that is very close to that of natural ones. To achieve this using covalent bond formation is challenging, because the reaction rates generally tend to drop significantly at low concentrations. Recently, Fyles and colleagues were able to circumvent this problem by cleverly using an increase in local concentration for activation of the building blocks by the chemical fuel and a subsequent intramolecular reaction for deactivation[14]. Another strategy reported by Walther and colleagues to gain temporal control (from minutes to days) over self-assembly processes relied on the transient change in pH induced by the hydrolytic cleavage of deactivators with varying chemical stability[28].

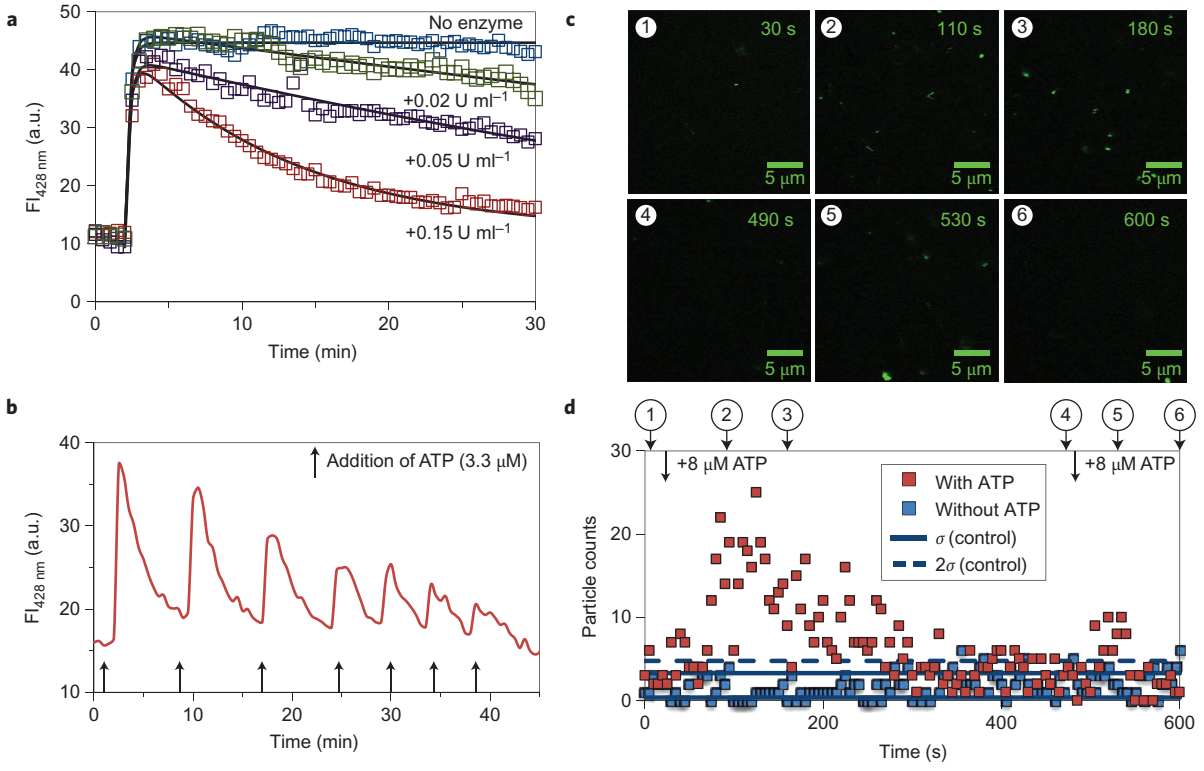


**Figure 2 | Transient formation of vesicles. a**, Fluorescent intensity (FI) at 428 nm as a function of time following addition of ATP (3 μM) to $C_{16}$TACN·$Zn^{2+}$ (10 μM) and DPH (2.5 μM) in the presence of different concentrations of potato apyrase. Experimental conditions: HEPES buffer (5 mM, pH 7.0); [$Ca^{2+}$] = 0.25 mM. All experiments were performed in triplicate (Supplementary Information, page 27). A representative data set is shown. Solid lines represent the best fits to model K1 (Supplementary Information, page 28). **b**, FI at 428 nm following seven repetitive additions of ATP (3.3 μM) to a solution of $C_{16}$TACN·$Zn^{2+}$ (10 μM) and DPH (2.5 μM) in the presence of potato apyrase (0.45 U $ml^{-1}$). **c**, Confocal images over time, showing the appearance and disappearance of fluorophore-bound vesicles in two cycles of ATP-fuelled vesicle formation and degradation. Samples were prepared using $C_{16}$TACN·$Zn^{2+}$ (25 μM), DPH (2.5 μM), potato apyrase (0.75 U $ml^{-1}$) and ATP (8 μM). **d**, Total number of fluorescent particle counts (calculated using ImageJ software; Supplementary Information, page 25) detected by confocal microscopy as a function of time (measured every 5 s) in the presence and absence of ATP. Numbers 1 to 6 denote the points corresponding to the images in **c**. Lines indicate standard deviations ($\sigma$ and $2\sigma$) for the background (no ATP). Experimental conditions in all cases: HEPES buffer (5 mM, pH 7), [$Ca^{2+}$] = 0.25 mM, slit width (ex/em) = 5/10 nm.

The next step forward towards functional dissipative assemblies requires the implementation of a functional property that is only operational as long as the system finds itself in the out-of-equilibrium state. It is well known that the apolar environment of aggregates such as micelles or vesicles can serve as a medium for chemical reactions that otherwise would not occur in water[29]. In our system, the apolar bilayer is present only in the out-of-equilibrium state, so we investigated the possibility of exploiting the vesicles as transient chemical reactors. The nucleophilic aromatic substitution reaction between 4-chloro-7-nitrobenzofurazan (NBD-Cl) and 1-octanethiol ($C_8$-SH) was chosen as the target reaction, because it was expected that the reported localization of NBD-Cl near the polar head groups in an aqueous solution of vesicles[30] and the solubilization of the apolar thiol in the bilayer would favour their reaction through spatial confinement (Fig. 3a,b). DLS measurement also confirmed that the presence of these two reactants did not affect the ability of ATP to induce aggregation (Supplementary Fig. 36). The reaction between NBD-Cl and $C_8$-SH in aqueous buffer resulted in the formation of just 9% of product (4-nitro-7-octylthiobenzofurazan (NBD-$SC_8$) after 30 min (Fig. 3c). The presence of only surfactant at 30 μM (below the CAC) or just ATP (5.5 μM) did not have any effect on the reaction (Fig. 3c and Supplementary Fig. 37). Considering that the concentration of ATP determines the level of vesicle formation (because of the well-defined ratio of ATP and $C_{16}$TACN·$Zn^{2+}$ in the assemblies), the effect of ATP concentration (2.5, 4.0 and 5.5 μM) on product formation was investigated first. Kinetic measurements followed by ultra performance liquid chromatography (UPLC) showed a gradual increase in the concentration of product, reaching constant values after about 25 min (Fig. 3c and Supplementary Fig. 34b). Different ATP concentrations clearly affected the overall yield of the reaction. Indeed, a linear relation was observed between the concentration of added ATP and the observed final yield after 30 min (Fig. 3d and Supplementary Fig. 35a).

To explain these results, kinetic model K2 was developed to simulate product formation by a bimolecular reaction in transient vesicles (Fig. 3b). This model is very similar to model K1, previously used to fit the decay curves, but contains additional equilibria between the reactants and products and the vesicles. In accordance with the experimental observation that the background reaction in the absence of vesicles hardly takes place, it was imposed that the bimolecular reaction occurs exclusively in the vesicles. Simulations were performed using parameters for vesicle formation and enzymatic ATP hydrolysis largely based on those previously obtained using model K1. It was assumed that the reaction product has a higher affinity for the vesicles than the reactants. This was based on a control experiment that showed that the addition of NBD-Cl and $C_8$-SH to vesicles pre-incubated with NBD-$SC_8$ yielded only a small amount of additional product (Supplementary Information, page 43). Product formation was calculated as a function of time for different ATP concentrations (but in the absence of enzyme), yielding profiles very similar to the experimental ones, and indicating that model K2 gives an accurate description of the kinetic processes occurring in the system (Fig. 3e). Importantly, a plot of the final concentration of product as a function of ATP concentration also provided a linear

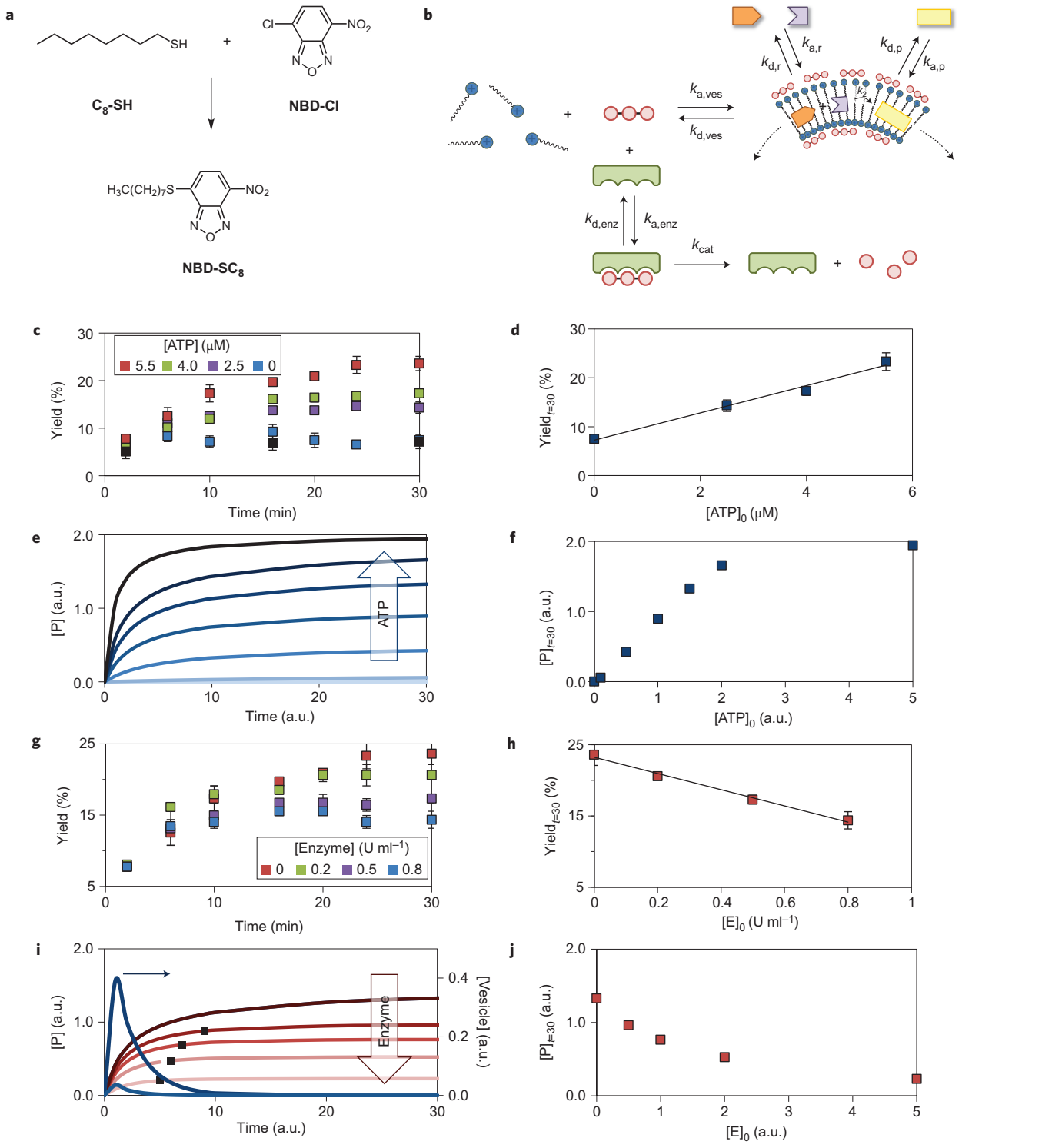


**Figure 3 | Product formation as a function of vesicle lifetime. a**, Scheme of the aromatic nucleophilic substitution reaction carried out in the vesicular system. **b**, Representation of the kinetic processes implemented in model K1. **c**, Yield (%) of the **NBD-SC$_8$** product as a function of time in a solution containing **C$_{16}$TACN·Zn$^{2+}$** (30 μM), reactants [**NBD-Cl**] = 1 μM, [**C$_8$-SH**] = 1.4 μM and different concentrations of ATP. Black points denote the reaction progress only in the presence of reactants in aqueous buffer solution without **C$_{16}$TACN·Zn$^{2+}$** and ATP. **d**, Yield (%) of the **NBD-SC$_8$** product as a function of ATP after a reaction time of 30 min. **e**, Simulated product formation as a function of time using model K2 for different initial concentrations of ATP. **f**, Simulated product formation at $t = 30$ as a function of initial concentration of ATP. **g**, Yield (%) of the **NBD-SC$_8$** product as a function of time in the presence of different concentrations of potato apyrase at a fixed ATP concentration (5.5 μM) in a solution containing **C$_{16}$TACN·Zn$^{2+}$** (30 μM) and reactants **NBD-Cl** (1 μM) and **C$_8$-SH** (1.4 μM). **h**, Yield (%) of the **NBD-SC$_8$** product as a function of enzyme concentration after a reaction time of 30 min. **i**, Simulated product formation (shades of red and brown) as a function of time using model K2 for different initial concentrations of enzyme (the brown arrow indicates increasing enzyme concentration), and calculated vesicle concentration (blue) for two different enzyme concentrations (0.5 and 5 U ml$^{-1}$, respectively). **j**, Simulated product formation at $t = 30$ as a function of initial enzyme concentration. Experimental condition in all cases: HEPES buffer (5 mM, pH 7), [$Ca^{2+}$] = 0.25 mM. Error bars in **c**,**d**,**g**,**h** denote standard deviation based on triplicate measurements.

correlation up to yields of 80% (Fig. 3f). Based on this model, our interpretation of the obtained results is that the amount of ATP dictates the number of vesicles formed and thereby determines how much of the hydrophobic reactants can be solubilized in the hydrophobic bilayer. Product inhibition explains why the yields level off, and suggests that the vesicles have to be regarded as reactors, not catalysts.

These results are interesting as they show how ATP—in an indirect manner—controls how much product is formed. Nevertheless, the key question is what would happen in the system under dissipative conditions. This final experiment was encouraged by the observation that the observed reaction kinetics under static conditions are comparable to the decay rate of the vesicles under dissipative conditions. Thus, product formation was measured by varying the enzyme concentration (0.2, 0.5 and 0.8 U $ml^{-1}$) while keeping the ATP concentration constant (5.5 μM) (Fig. 3g and Supplementary Fig. 35b). The kinetic profiles suggest that the reaction stops earlier as the enzyme concentration increases, resulting in a lower final yield after 30 min. A plot of the yield as a function of enzyme concentration indeed indicates a decrease in the final yield as enzyme concentration increases (Fig. 3h). This is an impressive correlation, in particular considering the complexity of the system.

For this system, we also performed a series of simulations using model K2 (this time with the enzymatic degradation pathway of ATP activated) to obtain a better understanding of the origin of this observation. Simulations were performed by varying only the enzyme concentrations and leaving all other parameters constant, including the initial concentration of ATP. For this case, plots of the calculated concentration of product as a function of time again gave profiles similar to the experimental ones (Fig. 3i). Most importantly, the final amount of generated product decreases as the enzyme concentration increases (Fig. 3j). The nonlinear correlation observed during the simulations (as compared to the experimental one) originates from the fact that the simulations allow the exploration of a much wider range of conditions, thus permitting a complete visualization of the trends. The black points in Fig. 3i indicate the time required to obtain 90% of the final amount of product. These points show that the reaction indeed slows down earlier as the enzyme concentration increases, which was also observed experimentally, albeit in a less evident manner. A plot of the calculated vesicle concentration as a function of time for two enzyme concentrations provides an insight into the origin of the observed effect (Fig. 3i). At lower enzyme concentrations, larger amounts of vesicles are formed, which decay over a longer period of time. This suggests the presence of a larger reaction volume, which explains why more product is formed. On the other hand, when a large amount of enzyme is present, the ATP hydrolysis rate is so high that a smaller number of vesicles are formed, which, in addition, also have a lower lifetime. This poses a limit to the amount of product that can be produced by the system. Evidently, the efficiency of this regulatory mechanism depends also on the reaction rate between two reactants in the vesicle. In our model we assumed a rapid reaction between the reactants in the vesicle. If this rate is actually slow, the lifetime of the vesicle becomes an even more important parameter. In any case, this is the first example in which the chemical output of a synthetic system is coupled to its lifetime and forms a significant step towards the design of chemical systems able to mimic the complex regulatory and communication pathways of natural systems.

In conclusion, we have shown the dissipative self-assembly of a vesicular nanoreactor that requires chemical fuel to maintain the functional out-of-equilibrium state. A novel strategy has been developed that relies on the transient stabilization of vesicles through noncovalent interactions between the surfactants and ATP, which acts as the chemical fuel. The noncovalent nature of the activation process allows dissipative self-assembly to occur in a much faster kinetic regime (minutes) compared to systems that rely on covalent bond formation. In addition, we also report on an important step towards functional dissipative self-assembly by showing for the first time that it is possible to couple chemical reactivity exclusively to the transient state of the system. This represents an entirely new way to control product formation by a chemical reaction and exemplifies the new possibilities offered by dissipative self-assembly. We anticipate that the described strategy will permit a rapid advancement from 'traditional' self-assembly under thermodynamic control towards the self-assembly of complex chemical systems with life-like properties, enabling a full exploration of their unique potential.

## Methods

See Supplementary Information for details of the synthesis and characterization of the surfactant **$C_{16}$TACN**.

**Determination of the CAC of the metallo-surfactant $C_{16}$TACN·$Zn^{2+}$.** Stock solutions (20 mM) of both **$C_{16}$TACN** (by accurate weighing) and $Zn(NO_3)_2$ in milli-Q water were mixed in a 1:1 ratio to obtain a 1 or 10 mM surfactant solutions of **$C_{16}$TACN·$Zn^{2+}$**. Stock solutions were prepared freshly each day before use.

The CAC of the surfactant in the presence of 1 equiv. $Zn^{2+}$ was determined both by fluorescence and UV–vis spectroscopy using procedures described in the literature[31,32].

*Fluorescence spectroscopy.* The fluorimetric determination[31] of the CAC involves the use of the hydrophobic probe **DPH**, which shows an increase in fluorescence intensity at concentrations higher than the CAC due to the formation of aggregates with an hydrophobic environment in which the hydrophobic fluorophore is solubilized. **DPH** was initially dissolved in THF to obtain a 1 mM stock solution. A 2.5 μl aliquot of this stock solution was added to a 1 ml cuvette containing aqueous HEPES buffer (5 mM, pH 7.0) to obtain a final **DPH** concentration of 2.5 μM. The fluorescence intensities after subsequent additions of the surfactant (**$C_{16}$TACN·$Zn^{2+}$**) were recorded after the signal had stabilized (3–5 min; Supplementary Fig. 4a). The excitation and emission wavelengths were 355 and 428 nm, respectively. The temperature was maintained at 37 °C. A CAC of 106 μM was determined by extrapolation of the last four points of the curve to a fluorescence intensity of zero (Supplementary Fig. 4b).

*UV–vis spectroscopy.* Determination of the CAC by UV–vis spectroscopy[32] was performed using the solubilization method of the hydrophobic dye **DPH** at 37 °C. **DPH** was initially dissolved in THF to obtain a 1 mM stock solution. A 2.5 μl aliquot of this solution was added to a 1 ml cuvette containing aqueous HEPES buffer (5 mM, pH 7.0) solution to obtain a final **DPH** concentration of 2.5 μM. Absorption spectra were recorded in the 250–450 nm range following additions of the **$C_{16}$TACN·$Zn^{2+}$** solution (20–400 μM) after stabilization of the signal (3–4 min; Supplementary Fig. 5a). The CAC value was determined from a plot of the ratio of absorbance at 377 and 401 nm (A377/A401) versus the logarithmic of the surfactant concentration (Supplementary Fig. 5b). A CAC value of 107 μM was determined by this method.

**Determination of the diffusion coefficient.** The translational diffusion coefficient of C153 was extrapolated from fluorescence correlation spectroscopy (FCS) analysis under excitation at 400 nm. FCS curves were calculated from the cross-correlation function of the fluorescence intensity fluctuations, over the mean intensity, collected in each detection channel. C153 dissolved in a buffer solution at 500 nM concentration was used for the calibration of the optical set-up. The diffusion coefficient of C153 (660 $\mu m^2\ s^{-1}$) was calculated from the rotational diffusion tensors under 'slip conditions' using the dimensions of a coumarin with a similar molecular structure[33].

The FCS curve of free-diffusion C153 in buffer was fitted with the following expression:

$$G(\tau) = \frac{1}{N}\left(1+\frac{\tau}{\tau_D}\right)^{-1}\left(1+\frac{\tau}{S^2\tau_D}\right)^{-1/2}$$

where $N$ is the average probe number in the focal volume, $\tau_D$ is the translational diffusion coefficient and $S$ is the laser beam shape factor ($S = z_0/\omega_0$, where $z_0$ and $\omega_0$ are respectively defined as the axial and lateral beam radius).

The FCS curves of C153 embedded in vesicular systems are fitted with a two-components free diffusion equation[34]:

$$G(\tau) = \frac{1}{N}\left[A\left(1+\frac{\tau}{\tau_{D1}}\right)^{-1}\left(1+\frac{\tau}{S^2\tau_{D1}}\right)^{-1/2} + (1-A)\left(1+\frac{\tau}{\tau_{D2}}\right)^{-1}\left(1+\frac{\tau}{S^2\tau_{D2}}\right)^{-1/2}\right]$$

where $\tau_{D1}$ is fixed to the value found for free-diffusion C153 in buffer, and $\tau_{D2}$ is the diffusion time assigned to C153 embedded in vesicular structures. Parameter $A$

represents the relative contribution of the free-diffusion term with respect to the second longer contribution. The acquisition time of these measurements was reduced to 15–20 s to avoid the detection of signals from large aggregates.

According to the Stokes–Einstein equation and the relation for the diffusion coefficient, $D = \omega_0^2/4\tau_D$, the hydrodynamic probe radius $R_h$ can be estimated from

$$R_h = \frac{K_B T \times 4\tau_{D2}}{6\pi\eta\omega_0^2}$$

where $K_B$ is Boltzmann's constant, $T$ is the absolute temperature (295 K) and $\eta$ is the solution viscosity.

The average diffusion coefficient and hydrodynamic radius of different samples are reported in Supplementary Table 2, confirming the results obtained from DLS data (for a comparison with DLS data see Fig. 1c).

All other synthetic procedure and experimental techniques are described in the Supplementary Information.

Received 29 September 2015; accepted 16 March 2016; published online 2 May 2016

## References


1. Kushner, D. J. Self-assembly of biological structures. *Bacteriol. Rev.* **33,** 302–245 (1969).
2. Gale, P. A. & Steed, J. W. (eds) *Self-assembly and Supramolecular Devices* (Supramolecular Chemistry: From Molecules to Nanomaterials Vol. 5, Wiley, 2012).
3. Mattia, E. & Otto, S. Supramolecular systems chemistry. *Nature Nanotech.* **10,** 111–119 (2015).
4. Karsenti, E. Self-organization in cell biology: a brief history. *Nature Rev. Mol. Cell Biol.* **9,** 255–262 (2008).
5. Whitesides, G. M. & Ismagilov, R. F. Complexity in chemistry. *Science* **284,** 89–92 (1999).
6. Fialkowski, M. *et al.* Principles and implementations of dissipative (dynamic) self-assembly. *J. Phys. Chem. B* **110,** 2482–2496 (2006).
7. Desai, A. & Mitchison, T. J. Microtubule polymerization dynamics. *Annu. Rev. Cell Dev. Biol.* **13,** 83–117 (1997).
8. Howard, J. *Mechanics of Motor Proteins and the Cytoskeleton* (Sinauer Associates, 2001).
9. Rizzoli, S. O. Synaptic vesicle recycling: steps and principles. *EMBO J.* **33,** 788–822 (2014).
10. Fletcher, S. P., Dumur, F., Pollard, M. M. & Feringa, B. L. A reversible, unidirectional molecular rotary motor driven by chemical energy. *Science* **310,** 80–82 (2005).
11. Ragazzon, G., Baroncini, M., Silvi, S., Venturi, M. & Credi, A. Light-powered autonomous and directional molecular motion of a dissipative self-assembling system. *Nature Nanotech.* **10,** 70–75 (2015).
12. Cheng, C. *et al.* Energetically demanding transport in a supramolecular assembly. *J. Am. Chem. Soc.* **136,** 14702–14705 (2014).
13. Cheng, C. *et al.* An artificial molecular pump. *Nature Nanotech.* **10,** 547–553 (2015).
14. Dambenieks, A. K., Vu, P. H. Q. & Fyles, T. M. Dissipative assembly of a membrane transport system. *Chem. Sci.* **5,** 3396–3403 (2014).
15. Krabbenborg, S. O., Veerbeek, J. & Huskens, J. Spatially controlled out-of-equilibrium host–guest system under electrochemical control. *Chem. Eur. J.* **21,** 9638–9644 (2015).
16. Boekhoven, J. *et al.* Dissipative self-assembly of a molecular gelator by using a chemical fuel. *Angew. Chem. Int. Ed.* **49,** 4825–4828 (2010).
17. Boekhoven, J., Hendriksen, W. E., Koper, G. J. M., Eelkema, R. & van Esch, J. H. Transient assembly of active materials fueled by a chemical reaction. *Science* **349,** 1075–1079 (2015).
18. Debnath, S., Roy, S. & Ulijn, R. V. Peptide nanofibers with dynamic instability through nonequilibrium biocatalytic assembly. *J. Am. Chem. Soc.* **135,** 16789–16792 (2013).
19. Pappas, C. G., Sasselli, I. R. & Ulijn, R. V. Biocatalytic pathway selection in transient tripeptide nanostructures. *Angew. Chem. Int. Ed.* **54,** 8119–8123 (2015).
20. Aida, T., Meijer, E. W. & Stupp, S. I. Functional supramolecular polymers. *Science* **335,** 813–817 (2012).
21. Warren, S. C., Guney-Altay, O. & Grzybowski, B. A. Responsive and nonequilibrium nanomaterials. *J. Phys. Chem. Lett.* **3,** 2103–2111 (2012).
22. Pezzato, C. & Prins, L. J. Transient signal generation in a self-assembled nanosystem fueled by ATP. *Nature Commun.* **6,** 7790 (2015).
23. Sasaki, R. & Murata, S. Aggregation of amphiphilic pyranines in water: facile micelle formation in the presence of methylviologen. *Langmuir* **24,** 2387–2394 (2008).
24. Koestereli, Z. & Severin, K. Fluorescence sensing of spermine with a frustrated amphiphile. *Chem. Commun.* **48,** 5841–5843 (2012).
25. Li, G., Zhang, S., Wu, N., Cheng, Y. & You, J. Spontaneous counterion-induced vesicle formation: multivalent binding to europium(III) for a wide-range optical pH sensor. *Adv. Funct. Mater.* **24,** 6204–6209 (2014).
26. Prins, L. J. Emergence of complex chemistry on an organic monolayer. *Acc. Chem. Res.* **48,** 1920–1928 (2015).
27. Cruz-Campa, I. *et al.* A novel class of metal-directed supramolecular DNA-delivery systems. *Chem. Commun.* 2944–2946 (2007).
28. Heuser, T., Steppert, A.-K., Molano Lopez, C., Zhu, B. & Walther, A. Generic concept to program the time domain of self-assemblies with a self-regulation mechanism. *Nano Lett.* **15,** 2213–2219 (2015).
29. Walde, P., Umakoshi, H., Stano, P. & Mavelli, F. Emergent properties arising from the assembly of amphiphiles. Artificial vesicle membranes as reaction promoters and regulators. *Chem. Commun.* **50,** 10177–10197 (2014).
30. Galinier, F., Bertorelle, F. & Fery-Forgues, S. Spectrophotometric study of the incorporation of NBD probes in micelles: is a long alkyl chain on the fluorophore an advantage? *C.R. Acad. Sci. Chim.* **4,** 941–950 (2001).
31. Zhang, X. C., Jackson, J. K. & Burt, H. M. Determination of surfactant critical micelle concentration by a novel fluorescence depolarization technique. *J. Biochem. Biophys. Methods* **31,** 145–150 (1996).
32. Yu, L., Zhang, H. & Ding, J. D. A subtle end-group effect on macroscopic physical gelation of triblock copolymer aqueous solutions. *Angew. Chem. Int. Ed.* **45,** 2232–2235 (2006).
33. Ryabov, Y. E., Geraghty, C., Varshney, A. & Fushman, D. An efficient computational method for predicting rotational diffusion tensors of globular proteins using an ellipsoid representation. *J. Am. Chem. Soc.* **128,** 15432–15444 (2006).
34. Chattoraj, S., Chowdhury, R., Ghosh, S. & Bhattacharyya, K. Heterogeneity in binary mixtures of dimethyl sulfoxide and glycerol: fluorescence correlation spectroscopy. *J. Chem. Phys.* **138,** 214507 (2013).


## Acknowledgements

This work was financially supported by the European Commission (grant MSCA 657486 to S.M.), COST Action CM1304 (to L.J.P.), the University of Padova (grant CPDA138148 to L.J.P.) and the Italian Ministry of Education and Research (grant PRIN2010C4R8M8 to C.F.). Full data are provided in the Supplementary Information. ESEM measurements were performed by C. Furlan at the CE.A.S.C. at the University of Padova. CryoTEM measurements were performed by E. Paccagnini in the Electron Microscopy Laboratory of the Department of Life Sciences at the University of Siena (director, P. Lupetti). The authors thank J. Chen for a critical assessment of the manuscript, M. Zerbetto for discussions on the FCS analysis and M. Zangrossi for preparation of the movies.

## Author contributions

S.M. and L.J.P. designed the experiments. S.M. performed all experiments, except for the FCS and confocal microscopy studies, which were performed by I.F. L.J.P. wrote models T, K1 and K2 and performed fitting and simulations. C.F. and P.S. were involved in data interpretation. L.J.P. wrote the manuscript and all authors commented on it.

## Additional information

Supplementary information and chemical compound information are available in the online version of the paper. Reprints and permissions information is available online at www.nature.com/reprints. Correspondence and requests for materials should be addressed to L.J.P.

## Competing financial interests

The authors declare no competing financial interests.